Report no. 00/20

Flutter and Forced Response of Mistuned Turbomachinery

M. S. Campobasso M. B. Giles

This report reviews the mathematical analysis of mistuned aeroelasticity in turbomachines, avoiding excessive mathematical complexity, and putting the emphasis on the physical interpretation of the mathematics. The aeroelastic behaviour can be analysed either by considering the motion of individual blades or by considering a sum of travelling wave modes. The modal viewpoint is shown to be most suitable when the degree of mistuning is small. On the other hand, the blade viewpoint is more natural when the structural mistuning is larger than the aerodynamic coupling, resulting in highly localised eigenmodes.

Asymptotic analyses are used to enlighten the physical mechanisms through which structural mistuning affects flutter and forced response, and their accuracy is assessed by comparison with the exact solution obtained by direct numerical computation. Numerical results illustrate the transition from travelling wave modes to localised vibration as the degree of mistuning increases, demonstrate the stabilising effect of mistuning on blade flutter and help explaining the dependence of the peak blade response on the order of the excitation in mistuned rotors. Monte Carlo simulations are carried out for randomly mistuned blades to draw conclusions on the expected effects of the mistuning.

Key words and phrases: turbomachinery aeroelasticity, alternate and random mistuning, mode localisation, perturbation theory

This research was supported by Rolls-Royce plc and EPSRC and this report is an expanded version of a paper presented at the ISUAAAT 2000 Conference in Lyon, France on September 4-8, 2000

Oxford University Computing Laboratory
Numerical Analysis Group
Wolfson Building
Parks Road
Oxford, England OX1 3QD
E-mail: sergio.campobasso@comlab.oxford.ac.uk

October, 2000

Contents

1 Introduction

Flutter and forced response of turbomachinery components such as fan, compressor and turbine blades are aeroelastic phenomena which may lead to dangerous mechanical failures if not properly accounted for in the design of the engine. Cyclic symmetry is a key assumption that is often used to dramatically simplify the aeroelastic analysis and design of bladed disks, as first shown in [10]. This is possible because the system can be modelled with a circulant matrix [4], whose properties allow one to investigate this problem by considering a single blade with a suitable periodic boundary condition, rather than the whole bladed disk. Unfortunately, probabilistic factors like manufacturing and material tolerances and unequal wear make questionable the assumption of cyclic symmetry and the validity of the results obtained with tuned analyses. As a matter of fact, the structurally tuned and mistuned assemblies can behave in a remarkably different fashion, the extent of these differences being quite problem dependent. Some trends, however, seem to be quite general and these include the evidence that (a) mistuning improves the flutter boundary [8, 7, 11]; (b) mistuning can either increase or reduce the blade forced response [8, 7, 5].

The use of perturbation techniques for turbomachinery aeroelasticity [1] has shown that both effects are qualitatively and quantitatively influenced by the ratio between the level of mistuning and the inter-blade coupling, which can be aerodynamic [11], mechanical [12, 13] or both [9]. The particular mistuning pattern can also play a significant role, and it has been shown that it can be optimised to achieve the stabilisation of a tuned unstable system [3].

Thus we see that there are three main reasons for studying the effects of structural mistuning on turbomachinery aeroelasticity: (a) accounting for the effects of the randomness in blade structural properties due to stochastic factors like manufacturing tolerances on the flutter boundaries (this could be done with a statistical approach, as in [2]); (b) assessing the applicability of selected mistuning patterns as a means of passive flutter control; (c) investigating the effects of both random and deliberate mistuning on the blade forced response.

In this report, the mechanisms through which alternate and random mistuning affect the free and forced response are enlightened by means of asymptotic expansions, matrix perturbation theory, exact numerical solution of the aeroelastic equations and Monte Carlo simulations. Particular emphasis is put on the importance of the ratio between mistuning level and aerodynamic coupling for both flutter and forced response. A careful analysis of alternately mistuned forced response is carried out, to explore its effects on the blade peak response when deliberately introduced in the system as a passive flutter control technique. The blade forced response in the presence of random mistuning is also addressed.

2 Model problem

To keep the analysis relatively simple so that the key issues can be examined in detail, we choose to consider a model problem in which there are N blades each of which undergoes a structural oscillation with a single degree-of-freedom $u_j(t), j = 1, 2, ..., N$. (Figure 1). Note that throughout this report we use periodic indices with modulus N so that $u_0 \equiv u_N$, $u_1 \equiv u_{N+1}$, and the statement $j = k$ is shorthand for $j = k \bmod N$.

After a suitable non-dimensionalisation, the equations of motion for the N blades are assumed to be of the form

$$\ddot{u}_j + (1 + \epsilon\sigma m_j)u_j = \epsilon \left(a_{-1}u_{j-1} + b_{-1}\dot{u}_{j-1} + a_0 u_j + b_0 \dot{u}_j + a_1 u_{j+1} + b_1 \dot{u}_{j+1}\right).$$

The left-hand side of the equation has the structural inertial and stiffness terms, with $\epsilon\sigma m_j$ being the structural mistuning. The right-hand side has the generalised forces due to aerodynamic coupling, with it being assumed that a blade only experiences a force due to its motion and the motions of its immediate neighbours on either side, and that the unsteadiness is of a sufficiently low frequency that the motion is well represented by just the displacement and velocity of each blade.

This model includes only mistuning due to variations in blade stiffness, but it is easily extended to handle mistuning due to variations in blade mass. It also does not consider structural coupling arising from inter-blade shrouds or disk flexibility, but these effects could easily be included in the aerodynamic 'stiffness' terms involving the displacements u_j and $u_{j\pm1}$.

It is convenient to write the equations of motion collectively as

$$\ddot{\boldsymbol{u}} + (I + \epsilon\sigma M)\boldsymbol{u} = \epsilon(A\boldsymbol{u} + B\dot{\boldsymbol{u}}), \tag{2.1}$$

with $\boldsymbol{u} = (u_1\ u_2\ \ldots\ u_N)^T$, M a diagonal matrix whose entries have zero mean and are normalised by their root mean square, A and B tridiagonal circulant matrices and σ a free parameter to control the ratio between the level of mistuning and the aerodynamic terms. Therefore the quantity $\epsilon\sigma$ is the root-mean-square of the deviations of the blade frequencies from the common tuned value, normalised by this same quantity.

A key feature of aeroelasticity in turbomachinery is that ϵ, a constant representing the order of magnitude of the structural mistuning and aerodynamic effects, is small; a value of 0.01 is representative. As a result, it is appropriate to use asymptotic analysis based on $\epsilon \ll 1$. When $\epsilon = 0$, we get simple uncoupled motion in which each blade vibrates with angular frequency $\omega = 1$ and its displacement can be expressed as the real part of a complex quantity,

$$u_j(t) = \mathcal{R}\left(c_j e^{i\omega t}\right),$$

or as the average of the complex quantity and its complex conjugate,

$$u_j(t) = \tfrac{1}{2}\left(c_j e^{i\omega t} + c_j^* e^{-i\omega t}\right).$$

In the general case with both aerodynamic coupling and structural mistuning, and without assuming that ϵ is small, the general behaviour is a sum of eigenmodes of the form

$$u_j(t) = e^{st} v_j,$$

where s is an eigenvalue and $\boldsymbol{v}$ is the corresponding eigenvector satisfying

$$\left((s^2+1)I+\epsilon(\sigma M-A-sB)\right)\boldsymbol{v}=0. \tag{2.2}$$

Taking the complex conjugate of this equation gives

$$\left((s^{*2}+1)I+\epsilon(\sigma M-A-s^*B)\right)\boldsymbol{v}^*=0,$$

so the complex conjugate s^* is also an eigenvalue, and its eigenvector is $\boldsymbol{v}^*$. Since the actual displacement is always a real quantity, the displacement can again be expressed either as the real part of the complex quantity or as the average of the quantity and its complex conjugate.

By defining $\boldsymbol{u}_0=\boldsymbol{u},\ \boldsymbol{u}_1=\dot{\boldsymbol{u}}$, equation (2.1) can also be written as

$$\frac{d}{dt}\begin{pmatrix}\boldsymbol{u}_0\\ \boldsymbol{u}_1\end{pmatrix}=\begin{pmatrix}0 & I\\ -I+\epsilon(A-\sigma M) & \epsilon B\end{pmatrix}\begin{pmatrix}\boldsymbol{u}_0\\ \boldsymbol{u}_1\end{pmatrix},$$

and by defining $\boldsymbol{v}_0=\boldsymbol{v},\ \boldsymbol{v}_1=s\boldsymbol{v}$, one obtains

$$s\begin{pmatrix}\boldsymbol{v}_0\\ \boldsymbol{v}_1\end{pmatrix}=\begin{pmatrix}0 & I\\ -I+\epsilon(A-\sigma M) & \epsilon B\end{pmatrix}\begin{pmatrix}\boldsymbol{v}_0\\ \boldsymbol{v}_1\end{pmatrix}.$$

In this form, one can use standard mathematical software such as MATLAB to obtain the $2N$ eigenvalues. Of particular interest is the pair of eigenvalues with the largest real component since these give the component of the general solution which grows fastest in time (if $\mathcal{R}(s)>0$) or decays to zero most slowly (if $\mathcal{R}(s)<0$). Thus it gives the asymptotic behaviour of the solution $\boldsymbol{u}(t)$ as $t\to\infty$.

Another important observation is that the sum of the $2N$ eigenvalues is equal to the trace (the sum of the diagonal elements) of the matrix, which is equal to $N\epsilon b_0$. A necessary requirement for stability is therefore that b_0 is negative. This also shows that the best that can be achieved through mistuning is that all $2N$ eigenvalues have the same negative real component equal to $\frac{1}{2}\epsilon b_0$.

Between the trivial case of identical blades without any coupling ($\epsilon=0$) and the most general one of mistuned blades with aerodynamic coupling ($\epsilon,\sigma,A,B,M\neq 0$), there are two important sub-cases to be considered: (a) tuned assemblies with aerodynamically coupled blades ($\epsilon,A,B\neq 0,\ \sigma=0$) and (b) mistuned assemblies with uncoupled blades ($\epsilon,\sigma,M\neq 0,\ A=B=0$). When the former group of modelling assumptions holds, the motion of the blades is usually analysed with a travelling wave formulation, discussed in the next section. In the latter sub-case, conversely, an individual blade representation is better suited, as the eigensolution of the aeroelastic problem foresees that each blade vibrates independently from the others. Under these circumstances, in fact, the eigenvalues of equation (2.2) are the mistuned natural frequencies of the blades, given by

$$s_j=i\omega_j=i\sqrt{1+\epsilon\sigma m_j}$$

and each eigenvector has only one nonzero entry, corresponding to the free motion of the blade it refers to.

3 Travelling wave representation

When dealing with spatially periodic systems like tuned rotors with aerodynamically coupled blades, it is common to use a Fourier series representation; in the context of turbomachinery aeroelasticity, this is usually referred to as a travelling wave representation.

The displacement of each blade is expressed as a sum of a number of circumferential Fourier modes,

$$u_j(t) = \sum_{k=1}^{N} \widehat{u}_k(t)\, e^{2\pi i j k/N}.$$

The amplitudes of the Fourier modes is given by the inverse mapping,

$$\widehat{u}_k(t) = \frac{1}{N} \sum_{j=1}^{N} u_j(t)\, e^{-2\pi i j k/N}.$$

It is convenient to express these two sets of equations in matrix-vector form as

$$\boldsymbol{u} = F\hat{\boldsymbol{u}}, \qquad \hat{\boldsymbol{u}} = F^{-1}\boldsymbol{u} = \frac{1}{N} F^H \boldsymbol{u},$$

where F^H denotes the Hermitian conjugate (complex conjugate transpose) of matrix F. Inserting the first of these into equation (2.1) and pre-multiplying the entire equation by F^{-1} yields the travelling wave form of the unsteady equations of motion,

$$\ddot{\hat{\boldsymbol{u}}} + (I + \epsilon\sigma\widehat{M})\hat{\boldsymbol{u}} = \epsilon(\widehat{A}\hat{\boldsymbol{u}} + \widehat{B}\dot{\hat{\boldsymbol{u}}}), \tag{3.1}$$

where

$$\widehat{M} = F^{-1}MF, \qquad \widehat{A} = F^{-1}AF, \qquad \widehat{B} = F^{-1}BF.$$

This has eigenmodes of the form

$$\hat{\boldsymbol{u}} = e^{st}\hat{\boldsymbol{v}},$$

where s is an eigenvalue and $\hat{\boldsymbol{v}}$ is the corresponding eigenvector satisfying

$$\left((s^2+1)I + \epsilon(\sigma\widehat{M} - \widehat{A} - s\widehat{B})\right)\hat{\boldsymbol{v}} = 0. \tag{3.2}$$

The attraction in using the travelling wave representation comes from the fact that $\widehat{A}$ and $\widehat{B}$ are both diagonal matrices. To prove this, we define the vectors $\boldsymbol{f}_k$ to be travelling wave modes of unit amplitude corresponding to the k^{th} column of matrix F. Since $F^H F = NI$, these vectors possess the important orthogonality property $\boldsymbol{f}_k^H \boldsymbol{f}_l = N\,\delta_{kl}$, where δ_{kl} is the Kronecker delta function which is unity when $k{=}l$ and zero otherwise.

Direct evaluation reveals that

$$A\boldsymbol{f}_l = \left(a_{-1}e^{-2\pi i l/N} + a_0 + a_1 e^{2\pi i l/N}\right)\boldsymbol{f}_l$$

and hence

$$\widehat{A}_{kl} \equiv \frac{1}{N}\, \boldsymbol{f}_k^H A \boldsymbol{f}_l = \left(a_{-1}e^{-2\pi il/N} + a_0 + a_1 e^{2\pi il/N}\right) \delta_{kl}.$$

Similarly,

$$\widehat{B}_{kl} \equiv \frac{1}{N}\, \boldsymbol{f}_k^H B \boldsymbol{f}_l = \left(b_{-1}e^{-2\pi il/N} + b_0 + b_1 e^{2\pi il/N}\right) \delta_{kl}.$$

The fact that $\widehat{A}$ and $\widehat{B}$ are diagonal means that in the absence of any structural mistuning the eigenmodes are pure travelling waves, and the eigenvalues are given by

$$s_k^2 + 1 = \epsilon(\widehat{A}_{kk} + s_k \widehat{B}_{kk}),$$

and so

$$s_k = \tfrac{1}{2}\epsilon \widehat{B}_{kk} \pm \sqrt{-1 + \epsilon \widehat{A}_{kk} + \tfrac{1}{4}\epsilon^2 \widehat{B}_{kk}}. \tag{3.3}$$

The negative root arising from the quadratic equation is the complex conjugate of one of the other positive roots, so we will not consider it further. When $\epsilon \ll 1$, the positive root can be expressed as an asymptotic series

$$s_k = i + \epsilon\lambda_k + O(\epsilon^2).$$

in which

$$\lambda_k = \tfrac{1}{2}(\widehat{B}_{kk} - i\widehat{A}_{kk}). \tag{3.4}$$

The real part of λ_k is

$$\mathcal{R}(\lambda_k) = \frac{1}{2}\left(b_o + (b_{-1}+b_1)\cos\beta_k - (a_{-1}-a_1)\sin\beta_k\right),$$

where $\beta_k \equiv 2\pi k/N$.

The left top and bottom plots in Figure 2 show the comparison between the exact and the asymptotic evaluation of the eigenvalues for two values of ϵ. The aerodynamic constants are $a_{-1} = -0.4443$, $a_0 = -0.3587$, $a_1 = 0.5296$, $b_{-1} = -0.0054$, $b_0 = -1.7000$, $b_1 = 1.5688$, corresponding to the first bending mode of a low-pressure turbine rotor with 20 blades (these values along with $\epsilon = 0.01$ hold for all figures presented in the report). Note that the imaginary components of all eigenvalues are clustered around i, because the aerodynamic coupling changes only slightly the *in vacuo* frequency of the blades. This effect increases with ϵ and is called *frequency shift*. The second and more important effect of the aerodynamic coupling is to introduce a small real component in the eigenvalues, whose sign determines the stability of the associated travelling mode. The opposite of this quantity is usually referred to as the *aerodynamic damping*. The eigenvalues of five modes are labelled in the left bottom plot in Figure 2. Negative aerodynamic damping corresponds to instability of the associated eigenmode and for this example, the 1^{st}, 2^{nd} and 3^{rd} Fourier modes are unstable (right top and bottom plots), whereas the 12^{th} is the most stable one. (The fact that only the first few modes are unstable is a frequent occurrence in the flutter of bladed rotors). After a transient phase in which the most stable modes rapidly decay to zero, the vibration of the assembly

is dominated by the least stable wave (k_0^{th}), whose eigenvalue has the biggest positive real part. In these conditions, the motion of the j^{th} blade is given by:

$$u_j(t) = \widehat{u}_k e^{i(\mathcal{I}(s_{k_0})t+\phi_j)} e^{\mathcal{R}(s_{k_0})t}$$

where $\phi_j = j\beta_{k_0}$. The phase between the motion of adjacent blades is usually referred to as the *inter-blade phase angle* and it is defined as $\alpha_j = \phi_{j+1} - \phi_j$. The expression above shows that in this case it is constant and equal to β_{k_0}. One should keep in mind, however, that this occurs only for tuned assemblies, whose eigenmodes are individual Fourier harmonics, each characterised by its own β_k. For mistuned assemblies, on the other hand, each eigenmode may result from the combination of more than one Fourier harmonic, as will be shown in the following sections.

To complete the travelling wave representation, we need to compute the elements of $\widehat{M}$. Expressing m_j as a Fourier series,

$$m_j = \sum_n \widehat{m}_n e^{2\pi i j n/N},$$

then

$$M\boldsymbol{f}_l = \sum_n \widehat{m}_n \boldsymbol{f}_{l+n},$$

and hence

$$\widehat{M}_{kl} \equiv \frac{1}{N}\boldsymbol{f}_k^H M \boldsymbol{f}_l = \sum_n \widehat{m}_n \delta_{k\,l+n} = \widehat{m}_{k-l}.$$

Because we started by assuming that the entries in M have zero mean, $\widehat{m}_0$ is zero. A uniform mistuning simply causes a slight shift in frequency which could be eliminated from the analysis by a minor change in the original non-dimensionalisation.

4 Alternate mistuning

In alternate mistuning the number of blades, N, is even and every second blade is identical. In the Fourier series representation just discussed, this corresponds to $\widehat{m}_{N/2}$ being the only non-zero Fourier component.

The presence of the off-diagonal term $\widehat{M}_{j\ j+N/2}$ leads to a coupling between travelling modes j and $j+N/2$, but they remain uncoupled from all other modes. Isolating the eigenvalue/eigenvector equations for these two modes alone, we have

$$\begin{pmatrix} s^2+1-\epsilon(\widehat{A}_{jj}+s\widehat{B}_{jj}) & \epsilon\sigma\widehat{m} \\ \epsilon\sigma\widehat{m} & s^2+1-\epsilon(\widehat{A}_{j'j'}+s\widehat{B}_{j'j'}) \end{pmatrix} \begin{pmatrix} \hat{v}_j \\ \hat{v}_{j'} \end{pmatrix} = 0, \qquad (4.1)$$

where for simplicity in notation we have omitted the subscript $N/2$ in $\widehat{m}_{N/2}$, and have defined $j' \equiv j+N/2$.

Setting the determinant of the matrix to zero, and letting s_j and $s_{j'}$ be the eigenvalues in the absence of mistuning, gives the quartic equation

$$(s-s_j)(s-s_j^*)(s-s_{j'})(s-s_{j'}^*) - \epsilon^2\sigma^2\widehat{m}^2 = 0, \qquad (4.2)$$

whose roots can be obtained numerically.

If $\epsilon \ll 1$ then the two roots near i have an asymptotic expansion of the form

$$s = i + \epsilon s^{(1)} + O(\epsilon^2),$$

which when substituted into (4.2) yields

$$-4(s^{(1)} - \lambda_j)(s^{(1)} - \lambda_{j'}) - \sigma^2 \widehat{m}^2 = 0,$$

and hence

$$s^{(1)} = \tfrac{1}{2}\left(\lambda_j + \lambda_{j'} \pm \sqrt{(\lambda_j - \lambda_{j'})^2 - \sigma^2 \widehat{m}^2}\right). \tag{4.3}$$

We call equation (4.3) a *single asymptotic* approximation, because it has been derived only assuming $\epsilon \ll 1$. There are a number of observations to be made about this result. The central one is that the solution varies significantly depending whether or not the level of mistuning σ is large relative to the difference between the aerodynamic terms λ_j and $\lambda_{j'}$.

If σ is much smaller, then a truncated Taylor series expansion of equation (4.3) provides the following *double asymptotic* approximation of the two roots

$$\begin{aligned} s^{(1)} &\approx \lambda_j - \tfrac{\sigma^2 \widehat{m}^2}{4(\lambda_j - \lambda_{j'})} \\ s^{(1)} &\approx \lambda_{j'} + \tfrac{\sigma^2 \widehat{m}^2}{4(\lambda_j - \lambda_{j'})} \end{aligned} \tag{4.4}$$

Thus, under these circumstances the eigenvalues are very close to their perfectly tuned values, and the effect of the mistuning is to slightly stabilise the less stable of the two modes, and at the same time slightly de-stabilise the other. Physically, what is happening is that the mistuning leads to a transfer of energy between the two travelling wave modes. If mode j is unstable and mode j' is stable, then energy is transferred from j to j' where it is then dissipated. This therefore improves the stability of mode j.

If σ is much larger than the aerodynamic terms, then the double asymptotic approximation of the two roots is

$$s^{(1)} \approx \pm \tfrac{1}{2} i\sigma\widehat{m} + \tfrac{1}{2}(\lambda_j + \lambda_{j'}) \mp \tfrac{1}{4} i \frac{(\lambda_j - \lambda_{j'})^2}{\sigma \widehat{m}}. \tag{4.5}$$

Hence, the eigenvalues are close to the pure mistuned values, but with a nearly equal offset due to the aerodynamic terms. Referring back to the coefficients of the original problem, one finds that

$$\tfrac{1}{2}(\lambda_j + \lambda_{j'}) = \tfrac{1}{2}(b_0 - i a_0).$$

Since b_0 is always negative for all applications of engineering interest this means that the mistuning has stabilised the system. To understand this physically, one needs to consider the associated eigenvectors which in the limit as $\lambda_j, \lambda_{j'} \to 0$ become $(1 \quad \pm 1)^T$. Thus the eigenmodes involve equal amounts of both travelling wave modes. What is happening is that the mistuning ensures a relatively rapid transfer of energy between

the two modes, and so one ends up with approximately the same energy level in each mode. The damping of the combined modes is therefore the average of their individual damping rates. The alternative blade viewpoint is that one mode consists primarily of even blades vibrating, the other the odd blades. In each case, the blades next to blades which are moving are almost stationary and so the only aerodynamic forces experienced are due to the blades' own motion as given by a_0 and b_0.

Figure 3 shows the eigenvalues (left plots) and the harmonic content of the least stable eigenmode (right plots) for the tuned and mistuned configuration. The least stable eigenmode of the tuned system consists only of the 2^{nd} Fourier mode ($\beta_2 = 36^0$), whereas that of the alternately mistuned assembly has both the 2^{nd} ($\beta_2 = 36^0$) and the 12^{th} ($\beta_{12} = 216^0$) ones, this latter being the most stable Fourier mode. Because of its beneficial contribution, the mistuned assembly has now become stable, since the eigenvalue corresponding to the least stable eigenmode now lies to the left of the imaginary axis (left bottom plot). As the level of mistuning increases, the cloud of eigenvalues splits in two and for high values of σ they are all clustered around the two frequencies of the softer and harder blade, with nearly constant aerodynamic damping for all modes. This is shown in Figure 4, where the sequence of the four plots in order of increasing σ also illustrates the transition from travelling wave to individual blade mode. The former holds for levels of mistuning equal or lower than the aerodynamic terms ($\sigma \leq 1$), whereas the transition to the latter mode is practically complete for $\sigma \approx 6$, which corresponds to a 3 % variation in the natural frequencies.

The stability parameter $\delta = \max \mathcal{R}(s)/\epsilon = \max \mathcal{R}(s^{(1)})$ is plotted versus σ in Figure 5. The first curve has been obtained calculating the exact eigenvalues of the matrix in equation (4.1), the second using the single asymptotic expansion given by equation (4.3) and the third and fourth ones using the double asymptotic expansion for dominant aerodynamic or mechanical terms (equations (4.4) and (4.5) respectively). From the exact stability curve, we observe that an unstable system achieves stability when the aerodynamic coupling and the level of mistuning are of the same order ($\sigma \approx 1$). For $\sigma \approx 6$ the system has nearly achieved its theoretical maximum stability ($\frac{1}{2}b_0$) and further increments of mistuning do not bring sensible improvements. These trends are quite well predicted by the single asymptotic analysis over the whole considered range of σ, whereas the two asymptotic curves corresponding to equations (4.4) and (4.5) are in good agreement with the exact values only where they were supposed to be valid, that is for low and high levels of mistuning, respectively.

5 Random mistuning

As in the previous section, we perform two asymptotic analyses of mistuning when its level is either very small or very large relative to the aerodynamic terms. In fact, each asymptotic analysis is doubly asymptotic, in that the first step, common to both, is to assume that $\epsilon \ll 1$ so that N eigenvalues can be expressed in asymptotic form as

$$s = i + \epsilon s^{(1)} + O(\epsilon^2).$$

Substituting this expression into equation (2.2) and neglecting the higher order terms yields the single asymptotic approximation

$$\left(s^{(1)}I - \tfrac{i}{2}(\sigma M - A - iB)\right)\boldsymbol{v} = 0, \tag{5.1}$$

while substituting it into equation (3.2) gives

$$\left(s^{(1)}I - \tfrac{i}{2}(\sigma \widehat{M} - \widehat{A} - i\widehat{B})\right)\hat{\boldsymbol{v}} = 0. \tag{5.2}$$

These two eigenvalue/eigenvector equations are now the subject of further asymptotic analysis using the theory presented in Appendix A.

5.1 relatively low mistuning

When the mistuning is small compared to the aerodynamic terms, we choose to use equation (5.2) with the matrix $\widehat{M}$ being regarded as a small perturbation to the diagonal matrix $\widehat{A}+i\widehat{B}$. Applying the theory in Appendix A, one obtains the following double asymptotic approximation of the eigenvalues

$$s_j^{(1)} \approx \lambda_j - \frac{\sigma^2}{4}\sum_{k\neq j}\frac{\widehat{M}_{jk}\widehat{M}_{kj}}{\lambda_j - \lambda_k}. \tag{5.3}$$

Now, using the relations previously established,

$$\widehat{M}_{jk}\widehat{M}_{kj} = \widehat{m}_{j-k}\widehat{m}_{k-j} = |\widehat{m}_{j-k}|^2,$$

since $\widehat{m}_{k-j} = \widehat{m}^*_{j-k}$. Also,

$$\frac{1}{\lambda_j - \lambda_k} = \frac{\lambda_j^* - \lambda_k^*}{|\lambda_j - \lambda_k|^2}, \quad \Longrightarrow \quad \mathcal{R}\left(\frac{1}{\lambda_j - \lambda_k}\right) = \frac{\mathcal{R}(\lambda_j) - \mathcal{R}(\lambda_k)}{|\lambda_j - \lambda_k|^2}.$$

Therefore, it follows that

$$\mathcal{R}(s_j^{(1)}) \approx \mathcal{R}(\lambda_j) - \sigma^2\sum_{k\neq j}\frac{|\widehat{m}_{j-k}|^2}{4}\,\frac{\mathcal{R}(\lambda_j) - \mathcal{R}(\lambda_k)}{|\lambda_j - \lambda_k|^2}.$$

Considering the index j corresponding to the least stable mode, the mode for which $\mathcal{R}(\lambda_j)$ is greatest, this result shows that the effect of the mistuning is always stabilising, since $\mathcal{R}(s_j^{(1)}) < \mathcal{R}(\lambda_j)$.

An interesting situation arises if the terms λ_k form a circle in the complex plane and so can be written as

$$\lambda_k = \lambda_0 + re^{i\theta_k}$$

with $\theta = 0$ corresponding to the least stable mode. In this case,

$$\frac{1}{\lambda_j - \lambda_k} = \frac{1}{r}\,\frac{1 - \cos\theta_k + i\sin\theta_k}{(1-\cos\theta_k)^2 + \sin^2\theta_k} = \frac{1}{2r}\left(1 + i\cot\frac{\theta_k}{2}\right).$$

and hence,

$$\mathcal{R}(s_j^{(1)}) \approx \mathcal{R}(\lambda_j) - \frac{\sigma^2}{8r} \sum_{k \neq j} |\widehat{m}_{j-k}|^2.$$

In addition, bearing in mind that the average level of mistuning is equal to zero, then Parseval's theorem gives that

$$\sum_{k \neq j} |\widehat{m}_{j-k}|^2 = \frac{1}{N} \sum_k m_k^2.$$

Thus, the amount by which the mistuning stabilises the least stable mode is independent of the pattern of mistuning in the particular case when the eigenvalues of the perfectly tuned system form a circle in the complex plane.

In the more general case, whether or not a particular mistuning pattern is better than another in stabilising the least stable mode at very low levels of mistuning will depend on how the undisturbed eigenvalues deviate from being circular. Unfortunately, the data published in the literature usually presents only the real part of the eigenvalues (since these determine the stability) and not the imaginary part (since these imply just a minor shift in frequency). More complete knowledge of the eigenvalues for actual fans, compressors and turbines is needed before any conclusion can be drawn regarding the optimum form of mistuning.

5.2 relatively high mistuning

When the mistuning is large compared to the aerodynamic terms, we choose to use equation (5.1) with the matrix $A+iB$ being regarded as a small perturbation to the diagonal matrix M. The unperturbed eigenvalues are $\frac{1}{2}\, i\sigma m_j$, therefore applying the perturbation theory gives the double asymptotic form

$$s_j^{(1)} \approx \tfrac{1}{2}\, i\sigma m_j + \tfrac{1}{2}(b_0 - ia_0) + \tfrac{i}{2\sigma} \sum_{k=j\pm 1} \frac{(a_{-1} + ib_{-1})(a_1 + ib_1)}{m_j - m_k}. \tag{5.4}$$

Considering only the real part of this, one obtains the following double asymptotic approximation of the eigenvalues

$$\mathcal{R}(s_j^{(1)}) \approx \tfrac{1}{2} b_0 - \tfrac{1}{2\sigma} \sum_{k=j\pm 1} \frac{a_{-1}b_1 + a_1 b_{-1}}{m_j - m_k}$$

This shows that at very high levels of mistuning the system is stable because of the dominance of the b_0 term which is negative in real applications. The physical interpretation of this is that at high levels of mistuning each blade vibrates on its own at its own natural frequency. The forces it experiences are due solely to its own motion, and these self-induced forces are always stabilising.

As the level of mistuning decreases, or equivalently the aerodynamic terms increase in strength, the aerodynamic forces cause the neighbouring blades to vibrate as well. The additional forces that this generates on the central blade may be stabilising or destabilising.

5.3 results

The random mistuning pattern in the left plot of Figure 6 has been used to solve the aeroelastic problem as given by equation (2.2) and the left top plot of Figures 7 and 8 shows the cloud of eigenvalues for an assembly with low and high level of random mistuning, respectively. By comparing them, one can notice how the loss of cyclic symmetry breaks the regular pattern of the tuned eigensolution. The harmonic content, the blade amplitudes of oscillation and the inter-blade phase angle α for the least stable eigenmode are provided in the top right, left bottom and right bottom plots, respectively. When the level of mistuning is low (Figure 7), the harmonic content is similar to the tuned one with a single travelling wave, indicating that the motion is still characterised by the dominance of a single Fourier mode ($\beta_2 = 36^0$). This is also reflected by the fact that the blade amplitudes of oscillation and inter-blade phase angles are nearly constant. Conversely, when the level of mistuning is high (Figure 8), the modal analysis of the least stable eigenvector reveals the presence of many Fourier modes. This corresponds to the localisation of the vibration to a few blades and to large variations of the inter-blade phase angle.

The evolution of the cloud of eigenvalues for increasing $\sigma's$ is displayed in Figure 9. The regularity of the tuned cloud is progressively broken as the level of mistuning increases. However the transition from travelling wave to individual blade mode takes place slower than with alternate mistuning. For example, the level of mistuning corresponding to $\sigma = 6$ is enough to equalise the damping of all eigenmodes in the alternate mistuning case (right bottom plot of Figure 4), whereas the damping of the eigenmodes is not yet as constant for the same amount of random mistuning (right bottom plot of Figure 9). Nevertheless the eigenmodes of the randomly mistuned system for $\sigma = 6$ correspond to the localisation of the vibration to a few blades. All this indicates that the vibration of the system does occur neither in the travelling wave nor in the individual blade mode, but rather in an intermediate form. The threshold σ above which the transition to individual blade mode is complete, depends both on the particular mistuning pattern and the shape of the cloud of tuned eigenvalues.

In order to compare the $\sigma - \delta$ stability curve for random and alternate mistuning and to make the results of the analysis represent the average effects of the randomness, a Monte Carlo simulation has been carried out by performing 1000 calculations with different random matrices M. The results plotted in Figure 10 correspond to the central 80 %, omitting the 10 % of the results with the best and worst stability and they show that mistuning always improves the stability of the assembly. However different patterns have different stabilising strength depending on the ratio between aerodynamic coupling and mistuning level. When the latter is lower or of the same order of the former one, the random distribution of blade stiffness is more effective than the alternate pattern, as proved by the fact that the stability band with random mistuning is below the stability curve with purely alternate mistuning for $0 < \sigma < 2$. On the other hand, when the level of mistuning is higher than the aerodynamic coupling, alternate mistuning is more effective than random mistuning. The stability band for random-alternate mistuning refers to a particular type of deliberate mistuning which can be obtained from any given

random pattern by first sorting the blades in order of increasing stiffness and then filling first the odd numbered slots in the disk and then the even ones. This produces a set of blades whose frequency alternates between low and high values. A random pattern and its random-alternate counterpart are given in Figure 6. We consider this type of mistuning both because of the stabilising properties shown by alternate mistuning and because of the ease by which it could be achieved in practice, since it only requires the measurement of the natural frequency of the blades before assembling them in the disk. The results of the statistical analysis provided in Figure 10 show that the stabilisation achieved with this pattern of mistuning is always greater than with the other two types of mistuning and this may suggest the use of the random-alternate rearrangement as a simple device for improving the flutter stability of those systems characterised by low aerodynamic coupling. A final remark on the results of these Monte Carlo simulations is that the vibration of the randomly mistuned assembly in the individual blade mode does not occur before $\sigma = 10$, which represents a pessimistic upper bound for the current manufacturing tolerances. For several mistuning patterns the individual blade mode did not occur before $\sigma's$ as high as 50.

Figure 11, shows the random and the random-alternate mistuning patterns that give the worst and the best stability for $\sigma = 10$. The best random-alternate is the closest to the purely random pattern, whereas the worst random is the farthest one. mainly because of the small difference between the frequency of blades 3 and 4 and blades 7 and 8.

An analogous Monte Carlo analysis has been carried out to assess the accuracy of the single (equation (5.1)) and double (equations (5.3) and (5.4)) asymptotic approximations of the aeroelastic problem. The asymptotic bands of aeroelastic stability are compared with the exact one determined with equation (2.2), in Figure 12. The agreement between the exact and the single asymptotic result is very good (the differences cannot be distinguished in the plot), the double asymptotic analysis for $\sigma \ll 1$ is acceptably accurate for low levels of mistuning and the double asymptotic analysis for $\sigma \gg 1$ gives poor results unless the level of mistuning is unrealistically high. The range of σ over which one has an acceptable agreement between the exact and the double asymptotic solution for high and low levels of mistuning is remarkably narrower than in the alternate mistuning case. In order to understand why this happens, let us consider the case of low mistuning with alternate and random mistuning. The double asymptotic stability is given by equations (4.4) and (5.3), respectively. In general, all Fourier modes are coupled when the rotor is randomly mistuned, whereas only the harmonics j and $j' \equiv j+N/2$ are coupled when the assembly is alternately mistuned. Therefore the perturbing terms $\frac{1}{\lambda_j - \lambda_k}$ in equation (5.3) can be quite large because of the small separation of adjacent eigenvalues, whereas the term $\frac{1}{\lambda_j - \lambda_{j'}}$ in equation (4.4) is smaller, because the eigenvalues j and j' are well separated one from the other, if the tuned cloud of eigenvalues is sufficiently regular. Consequently the range of σ over which the $O(\sigma^2)$ term remains small is much more limited in the random mistuning case. Similar arguments hold for the double asymptotic expansion for $\sigma \gg 1$.

6 Forced response

In forced response, equation (2.1) is modified through the addition of a prescribed periodic forcing term

$$\ddot{\boldsymbol{u}} + (I + \epsilon\sigma M)\boldsymbol{u} = \epsilon(A\boldsymbol{u} + B\dot{\boldsymbol{u}}) + \boldsymbol{f}(t). \tag{6.1}$$

The forcing term $\boldsymbol{f}(t)$ can be decomposed into a sum of components each of which has a particular frequency ω and an inter-blade phase angle β. Because of the linearity of the differential equation, the response to $\boldsymbol{f}(t)$ is equal to the sum of the responses to each of the individual components. Such components are normally referred to as *engine orders* ($E.O.$). By this term, one means the number of obstructions upstream or downstream of the rotor under investigation, which feels the resulting periodic circumferential variations of the flow field as a backward travelling excitation. Hence, the k^{th} harmonic is excited by the $(N-k)^{th}$ engine order in a tuned system. Therefore, from here onwards we analyse the case in which $\boldsymbol{f}(t)$ has just one such engine order.

Switching to the travelling wave representation, the forced response version of equation (3.1) is

$$\ddot{\hat{\boldsymbol{u}}} + (I + \epsilon\sigma\widehat{M})\hat{\boldsymbol{u}} = \epsilon(\widehat{A}\hat{\boldsymbol{u}} + \widehat{B}\dot{\hat{\boldsymbol{u}}}) + \hat{\boldsymbol{f}}(t), \tag{6.2}$$

with the elements of the vector $\hat{\boldsymbol{f}}$ being zero apart from the k^{th} element corresponding to the particular inter-blade phase angle of the forcing.

Making the substitutions

$$\boldsymbol{u}(t) = e^{i\omega t}\boldsymbol{v}, \quad \boldsymbol{f}(t) = e^{i\omega t}\boldsymbol{g}, \quad \hat{\boldsymbol{u}}(t) = e^{i\omega t}\hat{\boldsymbol{v}}, \quad \hat{\boldsymbol{f}}(t) = e^{i\omega t}\hat{\boldsymbol{g}},$$

then yields the following counterparts to equations (2.2) and (3.2),

$$\left((-\omega^2 + 1)I + \epsilon(\sigma M - A - i\omega B)\right)\boldsymbol{v} = \boldsymbol{g}. \tag{6.3}$$

$$\left((-\omega^2 + 1)I + \epsilon(\sigma\widehat{M} - \widehat{A} - i\omega\widehat{B})\right)\hat{\boldsymbol{v}} = \hat{\boldsymbol{g}}. \tag{6.4}$$

Either equation can be used to determine the blade forced response. For example, solving (6.3) yields $\boldsymbol{v}$, from which $\boldsymbol{u}(t)$ can be obtained.

If $|1-\omega^2| \gg \epsilon$ and $\sigma \approx 1$, the effect of the $O(\epsilon)$ terms in the two equations above is negligible, and the solution is

$$\boldsymbol{v} \approx \frac{1}{1-\omega^2}\,\boldsymbol{g},$$

and hence

$$\boldsymbol{u}(t) \approx \frac{1}{1-\omega^2}\,\boldsymbol{f}(t).$$

This equation holds for both tuned and not too heavily mistuned assemblies and it means that the blade response is independent of the engine order if the exciting frequency is far enough from the natural frequency of the blades.

On the other hand, if the exciting frequency is close to the natural frequency of the blades, then $1-\omega^2 = O(\epsilon)$ and the other $O(\epsilon)$ terms become significant. It is then more convenient to analyse separately the tuned and the mistuned cases.

6.1 tuned system

If there is no mistuning then, since $\widehat{A}$ and $\widehat{B}$ are diagonal, equation (6.4) can be solved to obtain

$$\hat{v}_k = \frac{\hat{g}_k}{1-\omega^2 - \epsilon(\widehat{A}_{kk} + i\omega\widehat{B}_{kk})}.$$

Making the substitution

$$\omega = 1 + \epsilon\omega^{(1)},$$

and ignoring terms which are $O(\epsilon^2)$ yields

$$\hat{v}_k = \frac{\hat{g}_k}{\epsilon(-2\omega^{(1)} - \widehat{A}_{kk} - i\widehat{B}_{kk})} = \frac{\hat{g}_k}{-2\epsilon(\omega^{(1)} + i\lambda_k)}.$$

If $\omega^{(1)}$ is treated as a variable, the peak response is

$$\hat{v}_k = \frac{\hat{g}_k}{-\epsilon\mathcal{I}(\widehat{A}_{kk} + i\widehat{B}_{kk})} = \frac{\hat{g}_k}{-2\epsilon\mathcal{R}(\lambda_k)}, \tag{6.5}$$

when

$$\omega^{(1)} = -\tfrac{1}{2}\mathcal{R}(\widehat{A}_{kk} + i\widehat{B}_{kk}) = \mathcal{I}(\lambda_k).$$

Equation (6.5) shows that the peak response of the tuned assembly is proportional to the reciprocal of the damping of the excited harmonic. Consequently, the difference between the response of the least and most damped harmonic decreases with increasing overall level of damping b_0. In particular, the response would be independent of the order of the excitation if the damping was constant for all modes. This condition is asymptotically approached for $b_0 \to -\infty$. In order to demonstrate the effect of different overall levels of damping on forced response, two stable tuned aeroelastic systems with low and high aerodynamic damping have been considered for the analyses presented in the following sections and their eigenvalues are plotted in Figure 13. These two spectra are obtained by shifting to the left the cloud of eigenvalues shown in the left top plot of Figure 2, to give $b_0 = -3$ and $b_0 = -8$.

Figure 14 shows the blade response γ of the tuned assembly with low damping ($b_0 = -3$) versus the forcing frequency ω and the *engine order* ($E.O.$), normalised by the maximum peak response. As expected, the maximum peak response occurs for the 18^{th} engine order, as this excites the least damped travelling wave (the 2^{nd}) and the minimum for the 8^{th}, as this excites the most damped travelling wave (the 12^{th}).

6.2 alternately mistuned system

When there is alternate mistuning, the forced response equation corresponding to equation (4.1) is

$$\begin{pmatrix} -\omega^2 + 1 - \epsilon(\widehat{A}_{kk} + i\omega\widehat{B}_{kk}) & \epsilon\sigma\widehat{m} \\ \epsilon\sigma\widehat{m} & -\omega^2 + 1 - \epsilon(\widehat{A}_{k'k'} + i\omega\widehat{B}_{k'k'}) \end{pmatrix} \begin{pmatrix} \hat{v}_k \\ \hat{v}_{k'} \end{pmatrix} = \begin{pmatrix} \hat{g}_k \\ 0 \end{pmatrix},$$

where for simplicity in notation we have again omitted the subscript $N/2$ in $\widehat{m}_{N/2}$, and have defined $k' \equiv k+N/2$. Note the term $\hat{g}_{k'}$ has been set to zero since we are considering forcing with an inter-blade phase angle corresponding to element k.

Making the substitution

$$\omega = 1 + \epsilon\omega^{(1)},$$

and ignoring terms which are $O(\epsilon^2)$ then yields

$$\begin{pmatrix} -2\omega^{(1)} - 2i\lambda_k & \sigma\widehat{m} \\ \sigma\widehat{m} & -2\omega^{(1)} - 2i\lambda_{k'} \end{pmatrix} \begin{pmatrix} \hat{v}_k \\ \hat{v}_{k'} \end{pmatrix} = \frac{1}{\epsilon} \begin{pmatrix} \hat{g}_k \\ 0 \end{pmatrix},$$

where λ_k and $\lambda_{k'}$ are as defined earlier in equation (3.4).

This has solution

$$\begin{pmatrix} \hat{v}_k \\ \hat{v}_{k'} \end{pmatrix} = \frac{1}{\epsilon D} \begin{pmatrix} -2\omega^{(1)} - 2i\lambda_{k'} \\ -\widehat{m} \end{pmatrix},$$

where

$$D = \det \begin{pmatrix} -2\omega^{(1)} - 2i\lambda_k & \widehat{m} \\ \widehat{m} & -2\omega^{(1)} - 2i\lambda_{k'} \end{pmatrix} = 4(\omega^{(1)} + i\lambda_k)(\omega^{(1)} + i\lambda'_k) - \widehat{m}^2.$$

Switching back into the blade viewpoint, it can be shown that the maximum response of any individual blade is equal to the greater of the two values given by

$$|\hat{v}_k \pm \hat{v}_{k'}| = \frac{|2\omega^{(1)} + 2i\lambda_{k'} \pm \widehat{m}|}{\epsilon |D|}. \tag{6.6}$$

The two plots in Figure 15 show that the alternately mistuned assembly has two peak responses for each engine order, one corresponding to resonance of the odd blades and one to resonance of the even ones. In both plots, the blade response is normalised by the maximum peak response of the tuned assembly. The peak response of the alternately mistuned system is higher than that of the tuned assembly for the 8^{th} engine order excitation and neighbouring ones, whereas it is lower for the 18^{th} and neighbouring ones. This can be explained considering the harmonic analysis of the peak blade response, shown in Figure 16. For each engine order, the harmonic content of the forced response has been normalised by the peak modal response of the tuned assembly. Note that although the inter-blade phase angle of the engine orders from 6 to 10 is that of the harmonics from 14 to 10 which are the more damped ones, there exist a remarkably high response of the harmonics from 20 to 4 too, which in turn are the less damped ones. This occurs because of the energy transfer between the harmonics k and $k+N/2$, which is triggered by the alternate mistuning. The damping of the resulting forced vibration is an average of the damping of the two coupled harmonics. As a consequence, the peak blade response of the alternately mistuned assembly is lower than the tuned one for the engine orders which excite directly the less damped harmonics thanks to the higher damping of the coupled ones. *Vice versa,* the alternately mistuned response is higher than the tuned one for the engine orders which excite directly the more damped harmonics because of the lower damping of the coupled ones

These mechanisms are quantitatively affected by the ratio between the level of mistuning and aerodynamic coupling. The ratio Γ_{max} between the maximum peak blade response of the alternately mistuned and the tuned assembly for all engine orders and for 5 values of σ is plotted in Figure 17. The curves have been calculated with the low damping tuned spectrum ($b_0 = -3$). Initially the differences between the tuned and mistuned peak response grow quite rapidly with the level of mistuning (curves for $\sigma = 0.5, 2.0$) and then more slowly for further increments (curves for $\sigma = 3.5, 5.0, 10$). This is due to the fact that the equalisation of the damping of the eigenmodes increases rapidly with the level of mistuning for $0 < \sigma < 4$ and more slowly thereafter, as the equalisation is nearly complete at $\sigma \approx 4$ (Figures 4 and 5). In these conditions the mistuned peak response becomes independent of the engine order and the curves for $\sigma > 3.5$ in Figure 17 are merely the reciprocal of the tuned peak response. They are still weakly varying with σ because of the decreasing stiffness of the softer blades, which leads to a slight growth in their response.

Figure 18 shows that the trends discussed above hold also for higher levels of aerodynamic damping, although with reduced strength. This is due to the higher uniformity of damping of the travelling waves.

The exact and asymptotic evaluations of Γ_{max} (equation (6.6)) for different levels of damping and mistuning are compared in the three plots of Figure 19, The agreement is in general quite good and this proves again the applicability of the asymptotic and perturbation techniques to turbomachinery aeroelasticity.

6.3 randomly mistuned system

All the results presented in this section refer to the random pattern of blade stiffness given in the left plot of Figure 6.

The forced response of the tuned rotor and of four selected blades for two levels of random mistuning versus the exciting frequency ω has been computed for the 8^{th} and 18^{th} engine order excitations and is plotted in Figure 20, in which all ordinates have been normalised by the maximum peak response of the tuned assembly. The left plots refer to the response of the tuned rotor and the other four to the response with random mistuning. There are several observations to be done. We first note that the mistuning of blade natural frequencies causes multiple peaks in the response, each corresponding to a particular blade frequency. As a consequence, resonance may now occur over a finite range of ω rather than at a single frequency like in the tuned assembly, and the potentially dangerous frequency span widens as the level of mistuning increases, since the difference between maximum and minimum blade frequency increases with σ. Comparing the tuned and mistuned response for $\sigma = 4$, shows that random mistuning increases the maximum peak response when the inter-blade phase angle of the excitation is that of the most damped travelling wave (8^{th} E.O.) and reduces it when the inter-blade phase angle is that of the least damped travelling wave (18^{th} E.O.), as in the alternate mistuning case. Additionally, the maximum peak response for this level of mistuning is not that of the softest blade (7^{th}), as visible in the centre bottom plot. The right plots show that the response becomes increasingly independent of the engine order as

σ increases. All these phenomena are due to the energy transfer among the travelling waves, as already discussed in the previous subsection.

The harmonic content of the peak blade response is shown in Figure 21. Unlike the alternate mistuning case, each engine order excites all harmonics. The dominant one is that which has the same inter-blade phase angle of the forcing, but there is always a contribution from all other harmonics too, in particular from the less damped ones (from 20 to 4). Therefore, the peak blade response with random mistuning is lower than the tuned one only for the engine orders which have the same inter-blade phase angle of the least damped travelling waves, since any contribution from the others can only increase the damping of the mistuned response. For all other engine orders, the peak response is higher than the tuned one, because the least damped harmonics are always involved in the response.

This is further emphasised in Figures 22 and 23 which provide the ratio Γ_{max} between the maximum peak response of the blades of the randomly mistuned assembly and the tuned peak response for all engine orders for five levels of mistuning σ and for two levels of aerodynamic damping. Figure 22 refers to the low damping case. Comparing the curves for $\sigma = 0.5, 2, 3.5$ with those in Figure 17, clearly shows that the maximum peak response with random mistuning is always equal or higher than that with alternate mistuning. This is due to the fact that the negative contribution of the least damped travelling waves to the overall damping is present for all engine orders when the rotor is randomly mistuned, and only for the fewer ones which have the inter-blade phase angle of the more damped travelling waves when the rotor is alternately mistuned. As σ increases, the energy transfer among travelling waves becomes stronger and it finally results in the response of the mistuned assembly being independent of the order of the excitation and the curves in Figure 22 tend to the reciprocal of the tuned response for very high $\sigma's$. As in the alternate mistuning case, these trends hold also for higher levels of aerodynamic damping, though with a reduced strength (Figure 23).

7 Conclusions

A comprehensive analysis of the effects of mistuning on turbomachinery aeroelasticity has been carried out.

The key factors affecting the free response of mistuned rotors are the topology of the tuned cloud of eigenvalues, the ratio between the level of mistuning and the inter-blade coupling and the mistuning pattern itself. When the structural mistuning is much lower or much higher than the aerodynamic terms, the free response of the system takes place in the travelling wave or in the individual blade mode, respectively. In the former case, the eigenmodes of the system are characterised by nearly constant amplitudes of oscillation and nearly constant inter-blade phase angle, whereas in the latter one the effect of the aerodynamic forces is only to provide a uniform damping for all eigenmodes, which consist of the vibration of individual blades. For the randomly mistuned assembly, however, the mistuning levels above which this state occurs are far beyond the worst current manufacturing tolerances, as proved by the Monte Carlo analyses. The vibration occurs in the travelling wave mode for the lower levels of mistuning and in an hybrid form for the higher levels. whose main feature is the localisation of the vibration to a small group of neighbouring blades.

The double asymptotic analyses prove that the effect of mistuning on the blade flutter is always stabilising in the limit of very low and very high mistuning-to-coupling ratios. When this parameter is small, the mistuning enhances the stability of the least stable travelling wave mode by transferring energy to the other more stable modes by which it is then dissipated and when it is high, the individual vibrating blades experience aerodynamic forces due only to their own motion, which are damping ones.

Both theoretical analysis and numerical results indicate that alternate mistuning is particularly effective in providing improved flutter stability for a given level of mistuning. This suggests the use of alternate mistuning as a measure for passive flutter control. The Monte Carlo simulations also demonstrate the improved stability that can be achieved by simply reordering a set of blades with varying properties due to manufacturing tolerances (random-alternate pattern). This method for passive flutter control would be particularly effective for assemblies with low aerodynamic coupling.

The energy transfer among travelling waves is also the key mechanism through which mistuning affects the forced response. The mistuned response depends on the damping of the harmonics involved by the excitation. Alternate mistuning couples only the k^{th} and the $(k + N/2)^{th}$ Fourier modes for an excitation of order $(N - k)$, whereas random mistuning involves all modes for any order of the excitation. In the latter case the least damped Fourier modes worsen the mistuned response for all orders of the excitations except for those which have its same inter-blade phase angle, since the damping of all the other modes is higher and brings a beneficial effect. In the alternate mistuning case, conversely, the response is lower than the tuned one for all engine orders $N - k$ such that the damping of the travelling wave k is lower than the damping of the travelling wave k'. Consequently the peak forced response with random mistuning is worse than the tuned response over a wider range of engine orders than the alternate mistuned is.

Structural mistuning also leads to peak splitting and to the widening of the frequency

range over which resonance may occur. These effects increase with the level of mistuning σ, whereas the amplifications and the reductions of the mistuned peak response with respect to the tuned one depend both on the ratio between mistuning and aerodynamic coupling and on the absolute level of damping, which influence the variations of damping associated to the travelling waves.

A final observation is that the computational costs of the analyses in this report are negligible, making the approach very suitable for design optimisation, or even for tailored assembly of blade sets during manufacturing. In particular, the single asymptotic models and the Monte Carlo simulations can be straightforwardly extended to 3D aeroelastic problems and introduced into everyday design practice, similarly to [6]. This is made possible by the fact that turbomachinery blades are usually designed keeping the structural modes well apart each from the other. Consequently, aeroelasticity analyses can be carried out considering a single degree-of-freedom per blade, corresponding to the structural mode under investigation.

References

[1] O.O. Bendiksen, January 1984. Flutter of mistuned turbomachinery rotors. *Journal of Engineering for Gas Turbines and Power*, **106**: 25–33.

[2] T.E. Smith C. Pierre and D.V. Murthy, May-June 1994. Localization of aeroelastic modes in mistuned high-energy turbines. *Journal of Propulsion and Power*, **10**(3): 318–328.

[3] E.F. Crawley and K.C. Hall, April 1985. Optimization and mechanisms of mistuning in cascades. *Journal of Engineering for Gas Turbines and Power*, **107**: 418–426.

[4] P.J. Davis, 1979. *Circulant matrices.* Wiley-Interscience.

[5] L.E. El-Bayoumi and A.V. Srinivasan, April 1975. Influence of mistuning on rotor-blade vibrations. *AIAA Journal*, **13**(4): 460–464.

[6] G. Kahl, 1997. Structural mistuning and aerodynamic coupling in turbomachinery bladings. In *Proceedings of the* 8^{th} *International Symposium on Unsteady Aerodynamics, Aeroacoustics and Aeroelasticity in Turbomachines.*

[7] K.R.V. Kaza and R.E. Kielb, November 1984. Flutter of turbofan rotors with mistuned blades. *AIAA Journal*, **22**(11): 1618–1625.

[8] R.E. Kielb and K.R.V. Kaza, October 1983. Aeroelastic characteristics of a cascade of mistuned blades in subsonic and supersonic flows. *Journal of Vibration, Acoustics, Stress and Reliability in Design*, **105**: 425–433.

[9] R.E. Kielb and K.R.V. Kaza, January 1984. Effects of structural coupling on mistuned cascade flutter and response. *Journal of Engineering for Gas Turbines and Power*, **106**: 17–24.

[10] F. Lane, January 1956. System mode shapes in the flutter of compressor blade rows. *Journal of the Aeronautical Sciences*, **23**(1): 54–66.

[11] C. Pierre and D.V. Murthy, October 1992. Aeroelastic modal characteristics of mistuned blade assemblies: Mode localization and loss of eigenstructure. *AIAA Journal*, **30**(10): 2483–2496.

[12] S.T. Wei and C. Pierre, October 1988. Localization phenomena in mistuned assemblies with cyclic symmetry part i: Free vibrations. *Journal of Vibration, Acoustics, Stress and Reliability in Design*, **110**: 429–438.

[13] S.T. Wei and C. Pierre, October 1988. Localization phenomena in mistuned assemblies with cyclic symmetry part ii: Forced vibrations. *Journal of Vibration, Acoustics, Stress and Reliability in Design*, **110**: 439–449.

Appendix A Eigenvalue/eigenvector perturbation theory

Consider the eigenvalues and eigenvectors defined by

$$(D + \epsilon P - \lambda I)\,\boldsymbol{u} = 0, \tag{A.1}$$

where D is a diagonal matrix with distinct eigenvalues and I is the identity matrix.

When $\epsilon = 0$, the eigenvalues are equal to the diagonal elements of D

$$\lambda_j^{(0)} = D_{jj}$$

and the eigenvectors are

$$\boldsymbol{u}_j^{(0)} = \boldsymbol{e}_j,$$

where $\boldsymbol{e}_j$ is the unit vector all of whose elements are zero except for the j^{th} which is unity.

When $\epsilon \ll 1$, the perturbed eigenvalues and eigenvectors can be expressed as asymptotic series,

$$\begin{aligned} \lambda_j &= \lambda_j^{(0)} + \epsilon\lambda_j^{(1)} + \epsilon^2\lambda_j^{(2)} + O(\epsilon^3), \\ \boldsymbol{u}_j &= \boldsymbol{e}_j + \epsilon \sum_{k\neq j} c_{jk}^{(1)} \boldsymbol{e}_k + O(\epsilon^2). \end{aligned}$$

Substituting these expressions into equation (A.1), and equating the terms which are $O(\epsilon)$, the k^{th} row, for $k \neq j$, yields

$$(\lambda_k^{(0)} - \lambda_j^{(0)})\, c_{jk}^{(1)} + P_{kj} = 0,$$

and hence

$$c_{jk}^{(1)} = \frac{P_{kj}}{\lambda_j^{(0)} - \lambda_k^{(0)}}.$$

Looking at the j^{th} row, the terms which are $O(\epsilon)$ yield

$$\lambda_j^{(1)} = P_{jj},$$

while the terms which are $O(\epsilon^2)$ yield

$$\lambda_j^{(2)} = \sum_{k\neq j} P_{jk} c_{jk}^{(1)} = \sum_{k\neq j} \frac{P_{jk}P_{kj}}{\lambda_j^{(0)} - \lambda_k^{(0)}}.$$

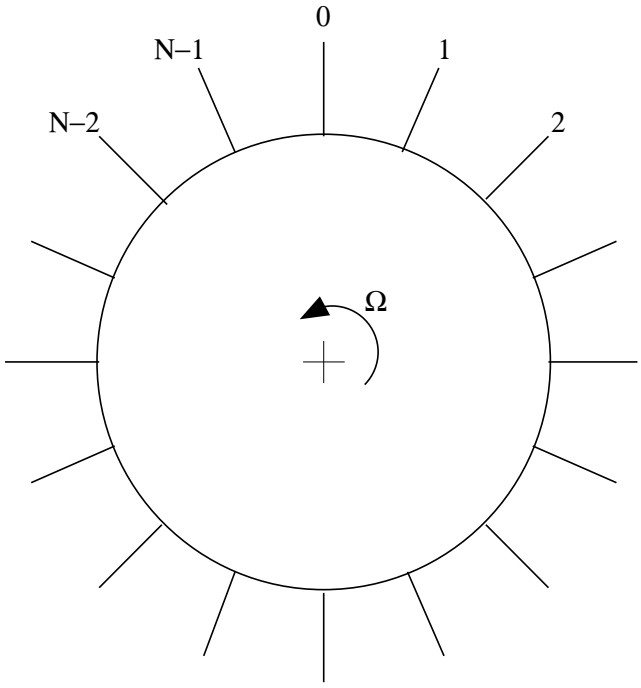

Figure 1: Model problem

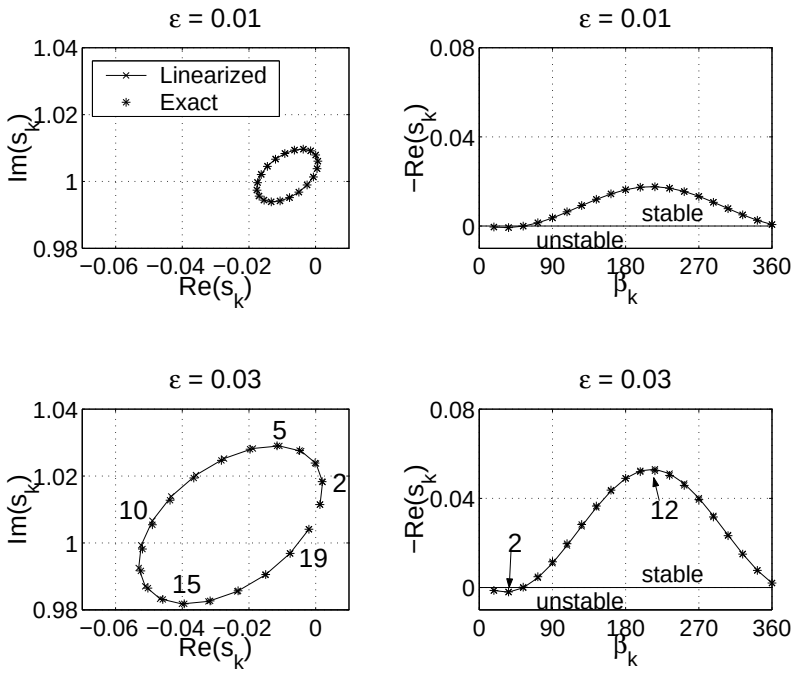

Figure 2: Exact versus linearised eigenvalues. ($N = 20, a_{-1} = -0.4443, a_0 = -0.3587$, $a_1 = 0.5296, b_{-1} = -0.0054, b_0 = -1.7000, b_1 = 1.5688$).

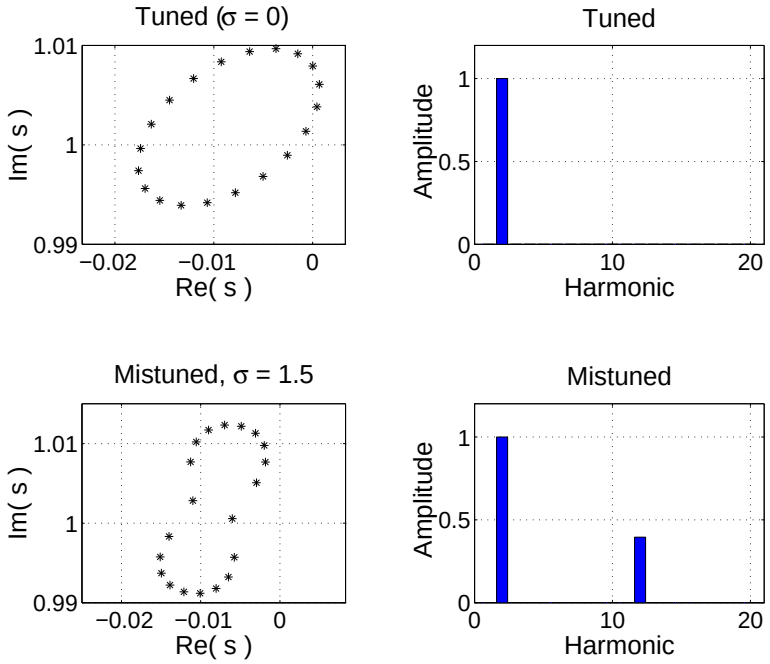

Figure 3: Coupling of travelling waves through alternate mistuning ($\epsilon = 0.01$).

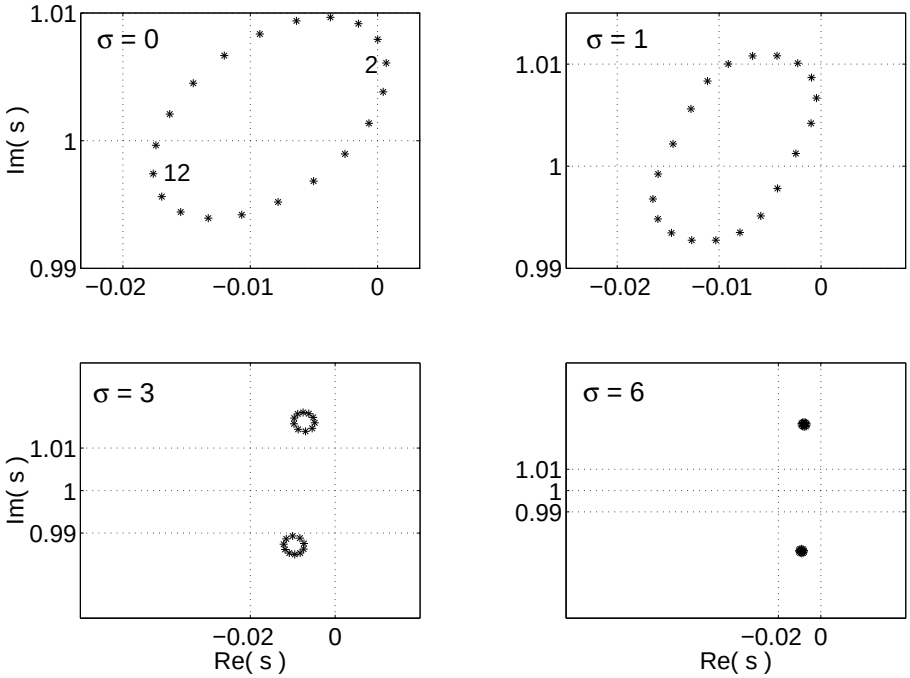

Figure 4: Effect of increasing amount of alternate mistuning.

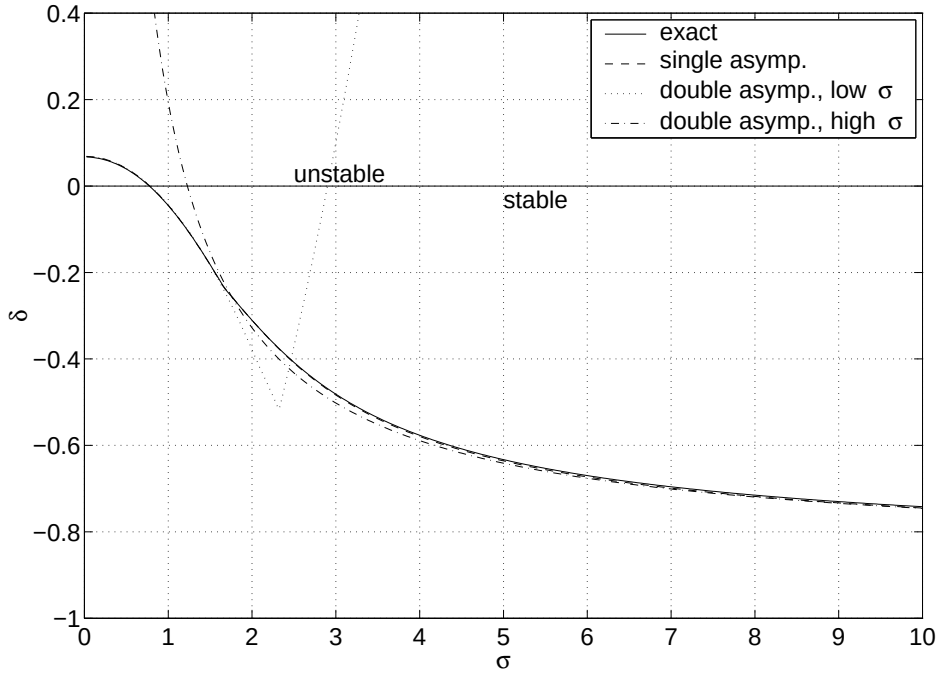

Figure 5: Aeroelastic stability versus level of alternate mistuning. Exact and asymptotic analyses.

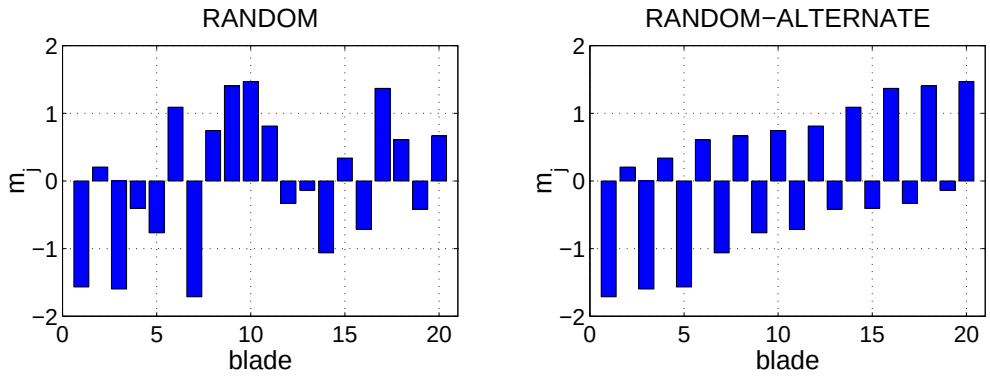

Figure 6: Random and random-alternate mistuning patterns of blade stiffness.

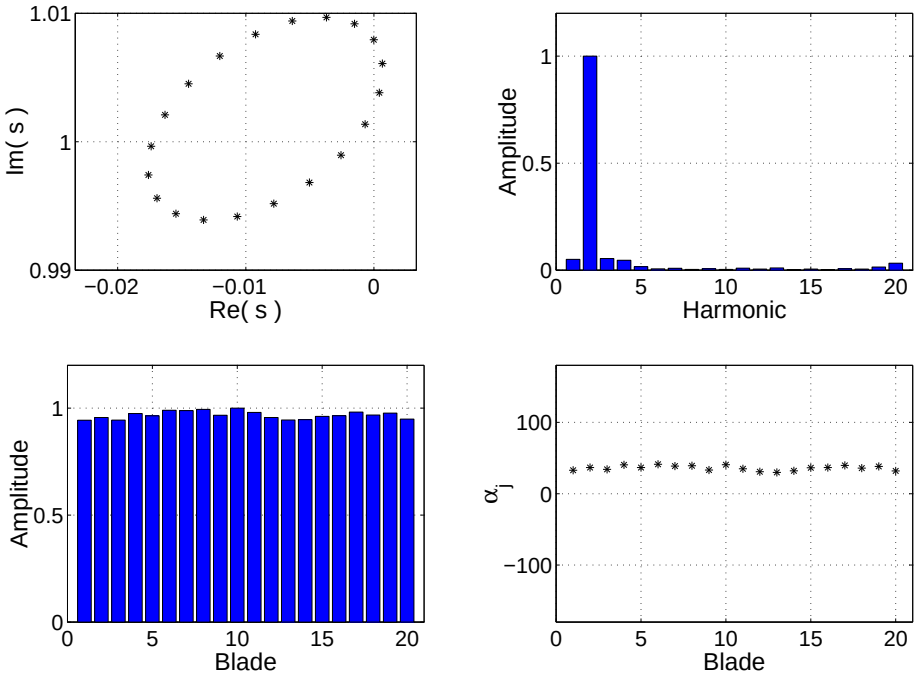

Figure 7: Eigenvalues and least stable eigenmode for an assembly with low level of random mistuning ($\sigma = 0.1$).

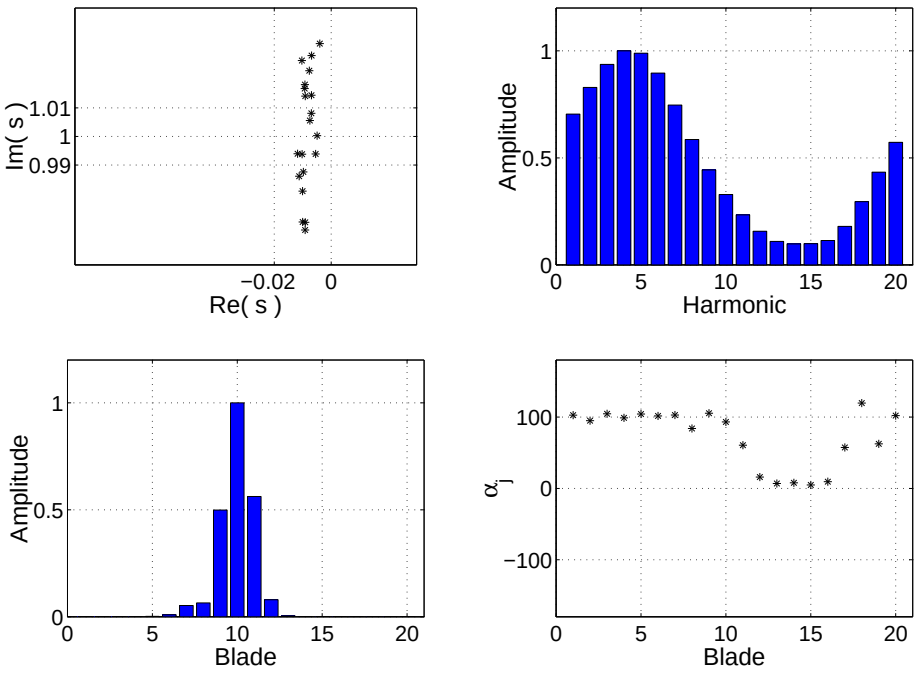

Figure 8: Eigenvalues and least stable eigenmode for an assembly with high level of random mistuning ($\sigma = 4.0$).

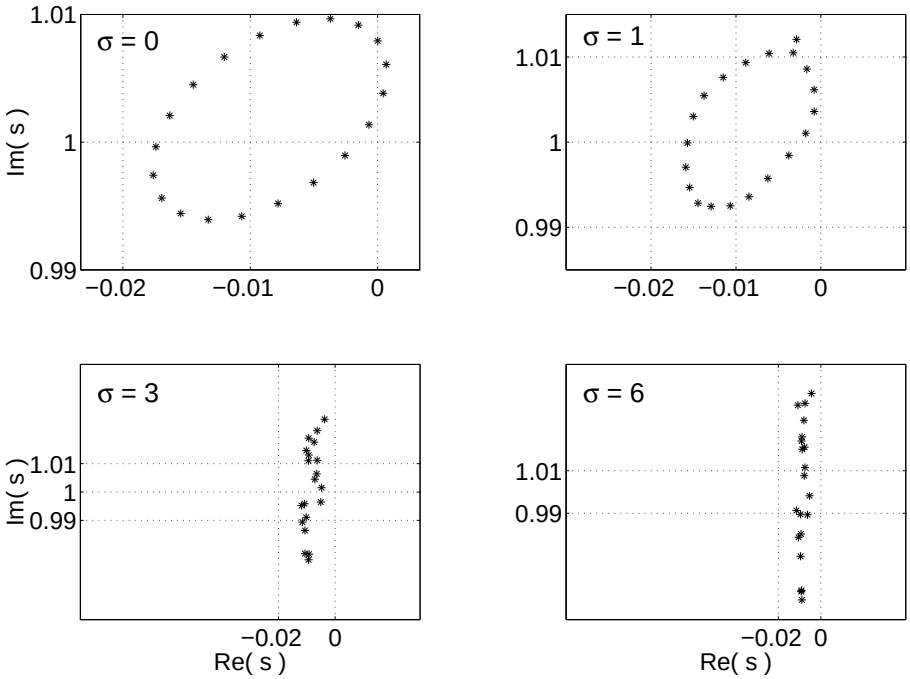

Figure 9: Effect of increasing amount of random mistuning.

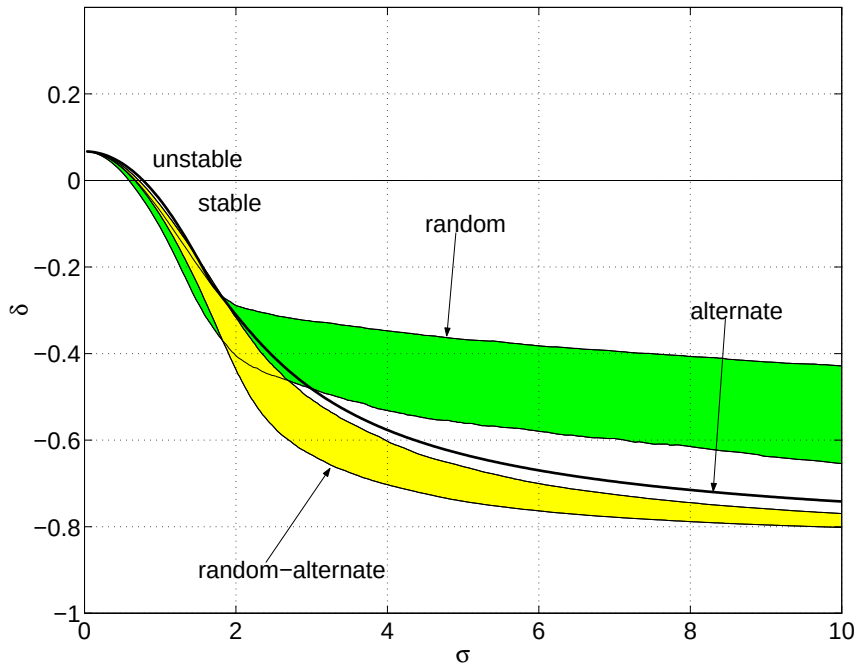

Figure 10: Aeroelastic stability versus level of alternate, random and random-alternate mistuning. Monte Carlo analysis.

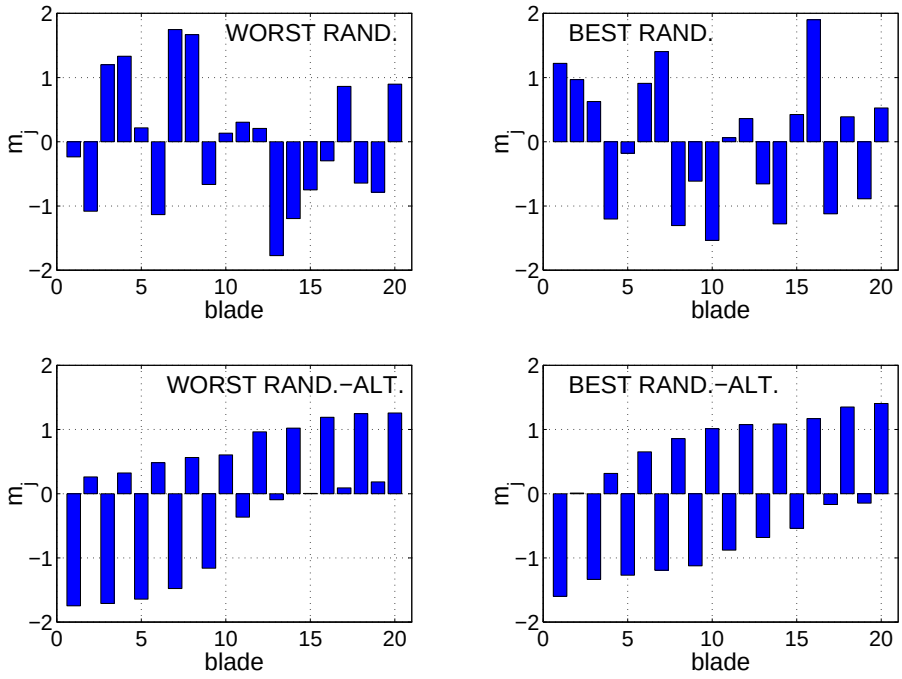

Figure 11: Blade stiffness patterns for worst and best stability with random and random-alternate mistuning. ($\sigma = 10$).

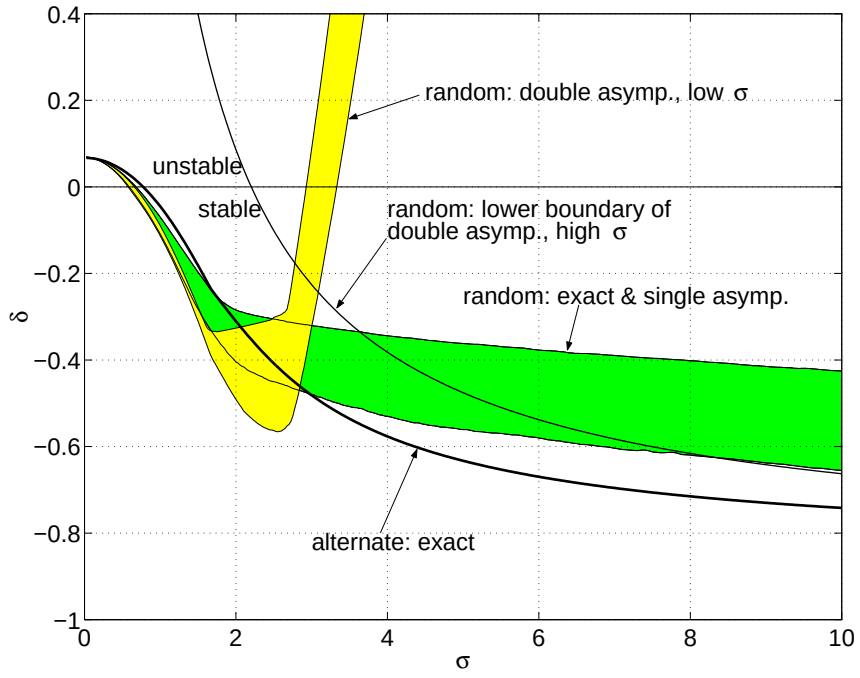

Figure 12: Exact and asymptotic aeroelastic stability versus level of random mistuning. Monte Carlo analysis.

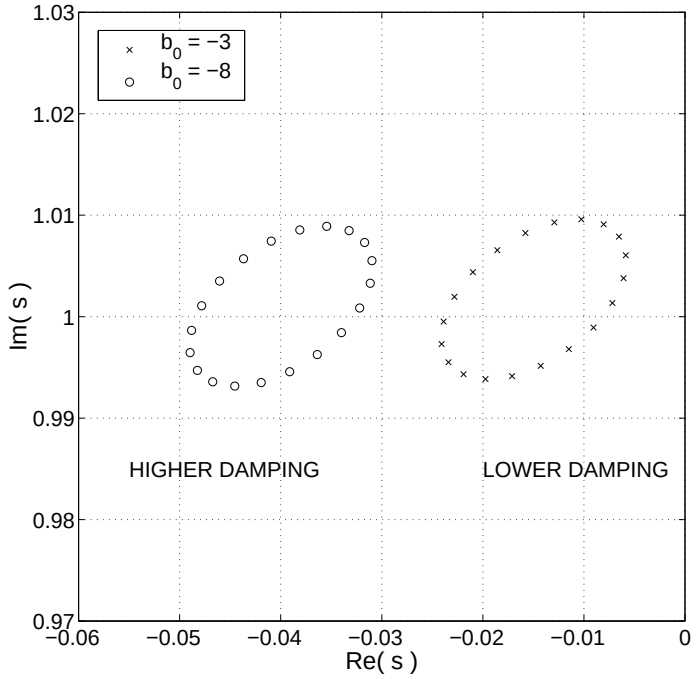

Figure 13: Tuned clouds of eigenvalues with different level of aerodynamic damping used for forced response analyses.

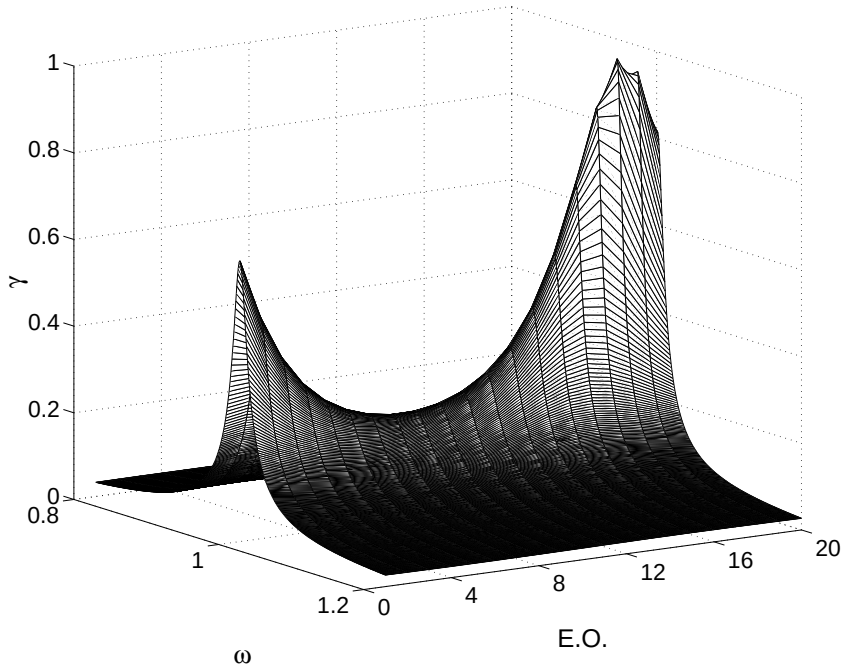

Figure 14: Blade response of tuned assembly ($b_0 = -3, \sigma = 0$).

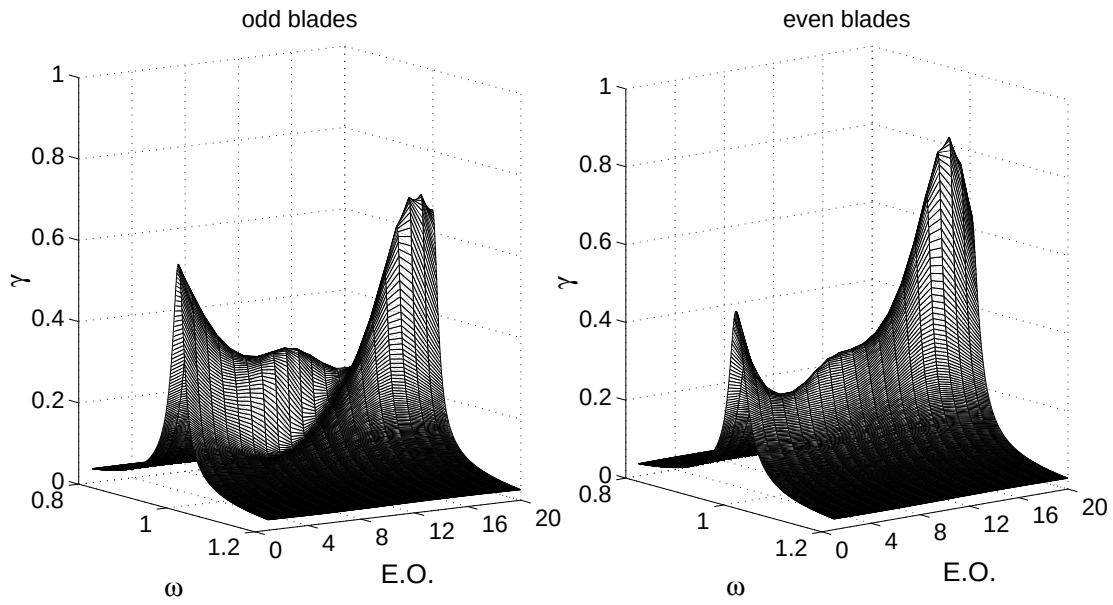

Figure 15: Blade response of alternately mistuned assembly ($b_0 = -3, \sigma = 1.5$).

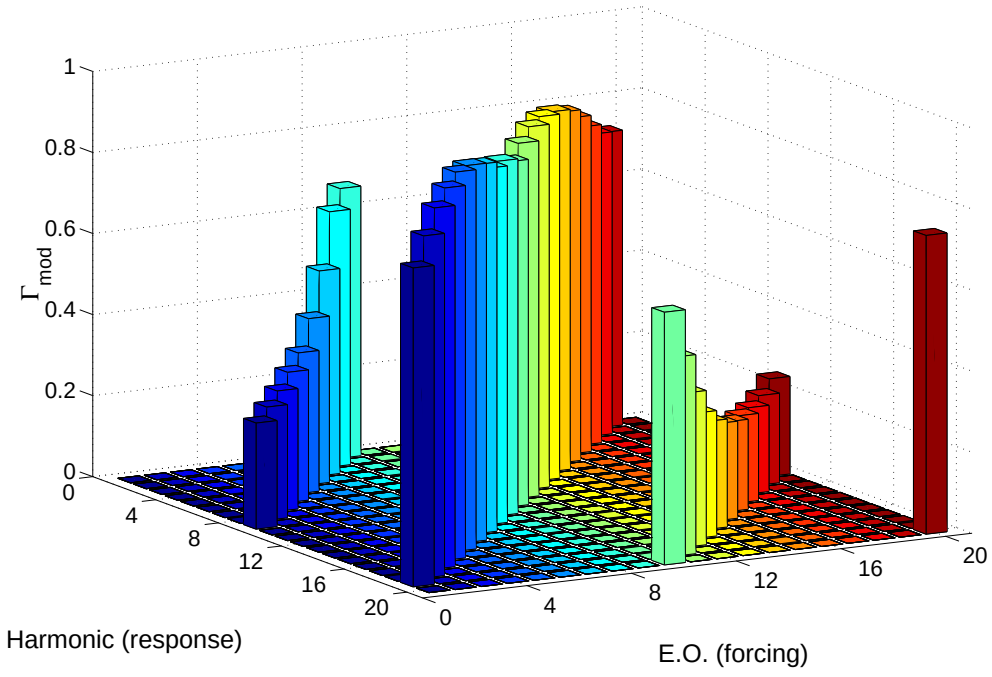

Figure 16: Harmonic content of peak blade response of the alternately mistuned assembly ($b_0 = -3, \sigma = 1.5$).

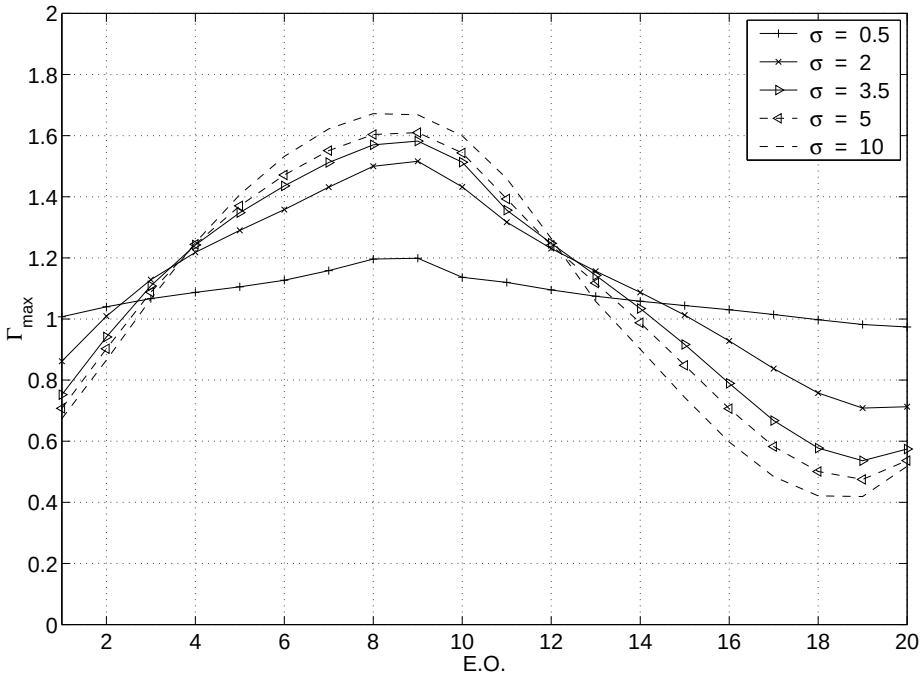

Figure 17: Maximum blade response of alternately mistuned assembly with low level of aerodynamic damping ($b_0 = -3$).

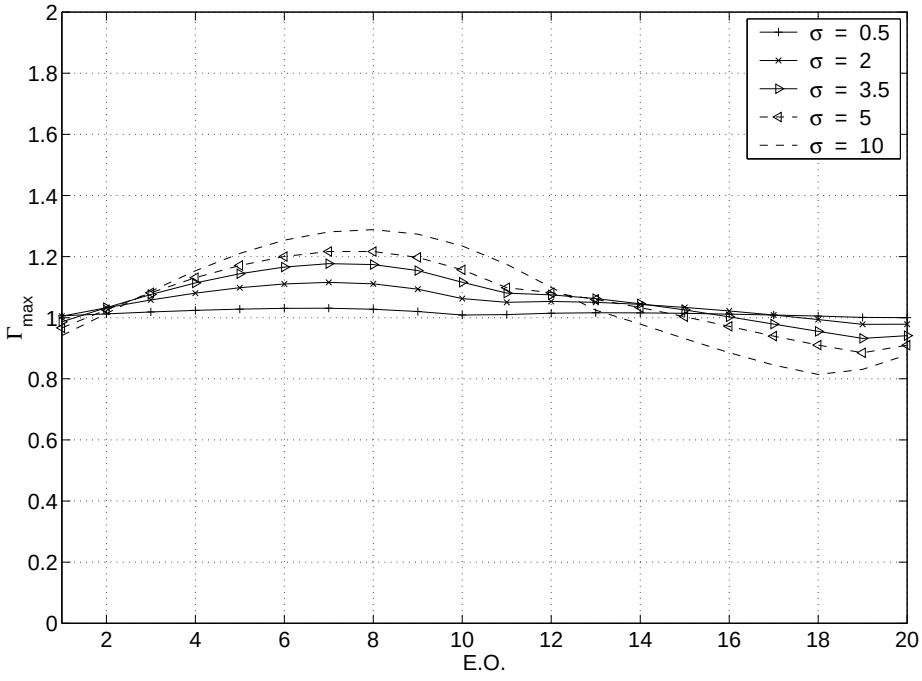

Figure 18: Maximum blade response of alternately mistuned assembly with high level of aerodynamic damping ($b_0 = -8$).

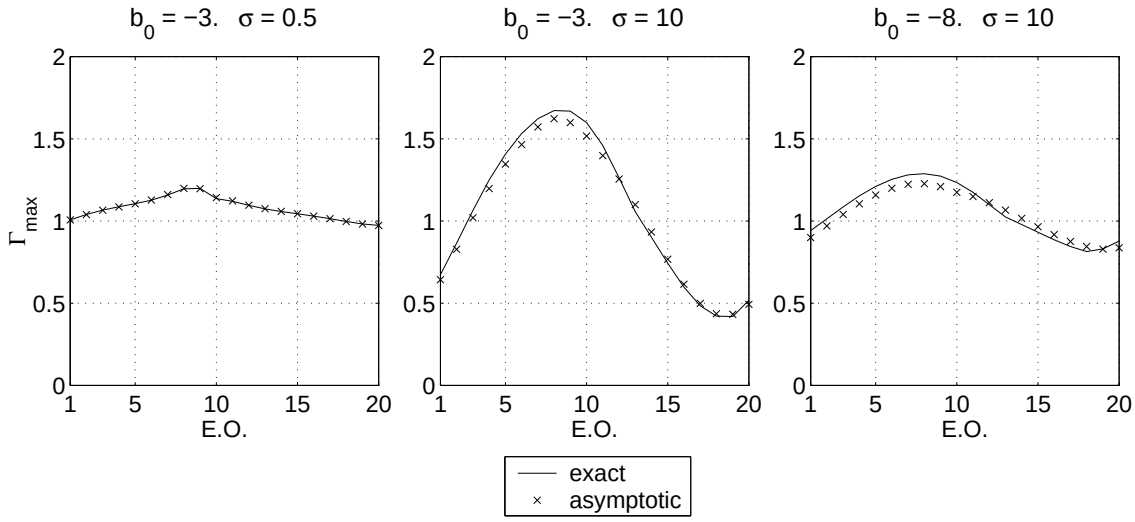

Figure 19: Exact and asymptotic predictions of blade peak response with alternate mistuning.

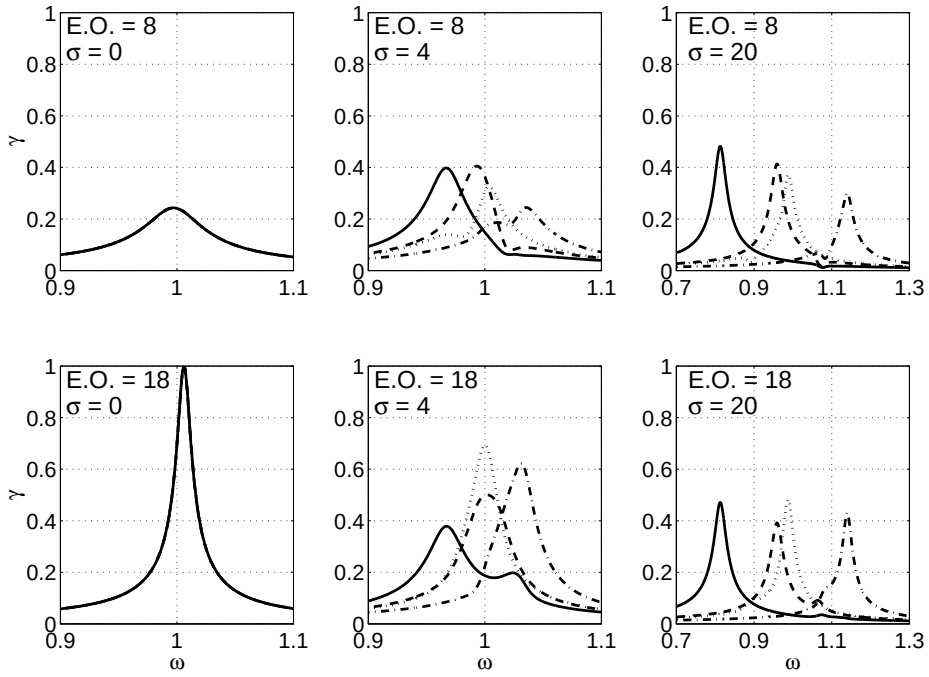

Figure 20: Blade response of randomly mistuned assembly for two engine orders and for different levels of mistuning. (—: blade 7, − −: blade 19, · · ·: blade 13, -.-.-: blade 10).

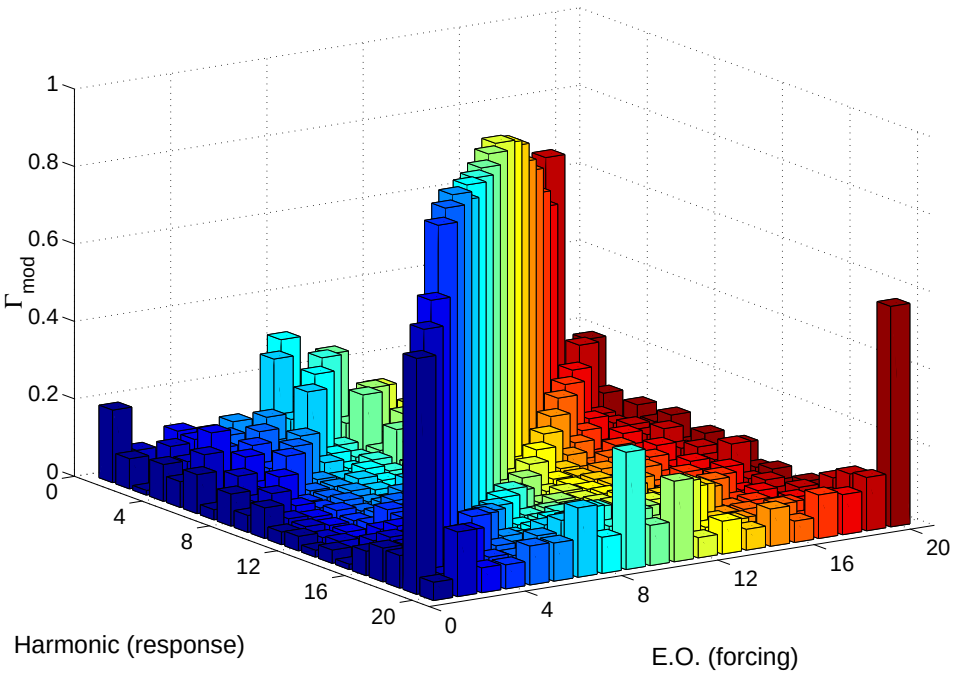

Figure 21: Harmonic content of peak blade response of a randomly mistuned assembly ($b_0 = -3, \sigma = 1.5$).

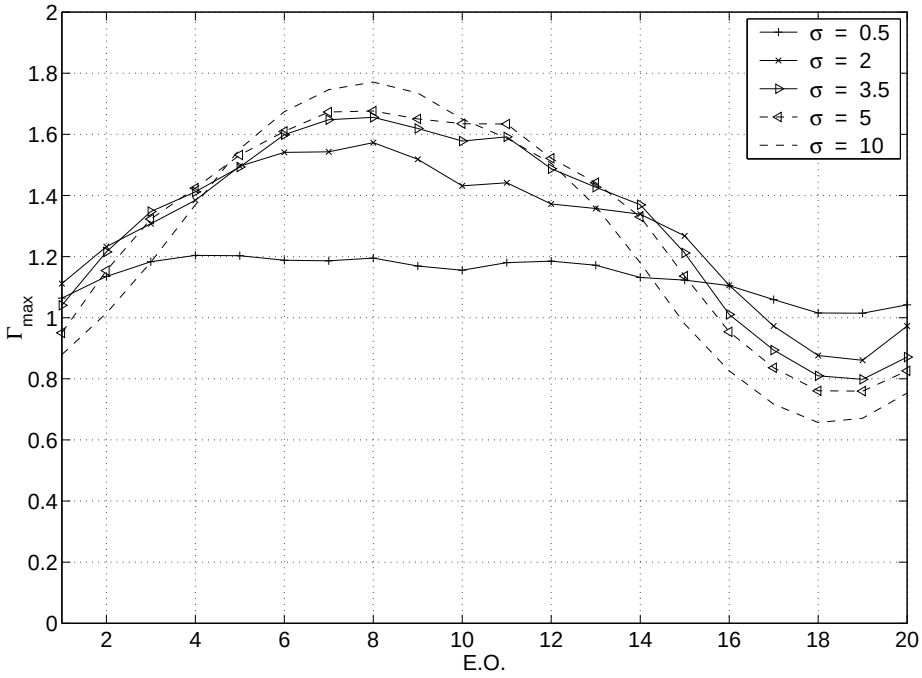

Figure 22: Maximum blade response of randomly mistuned assembly with low level of aerodynamic damping ($b_0 = -3$).

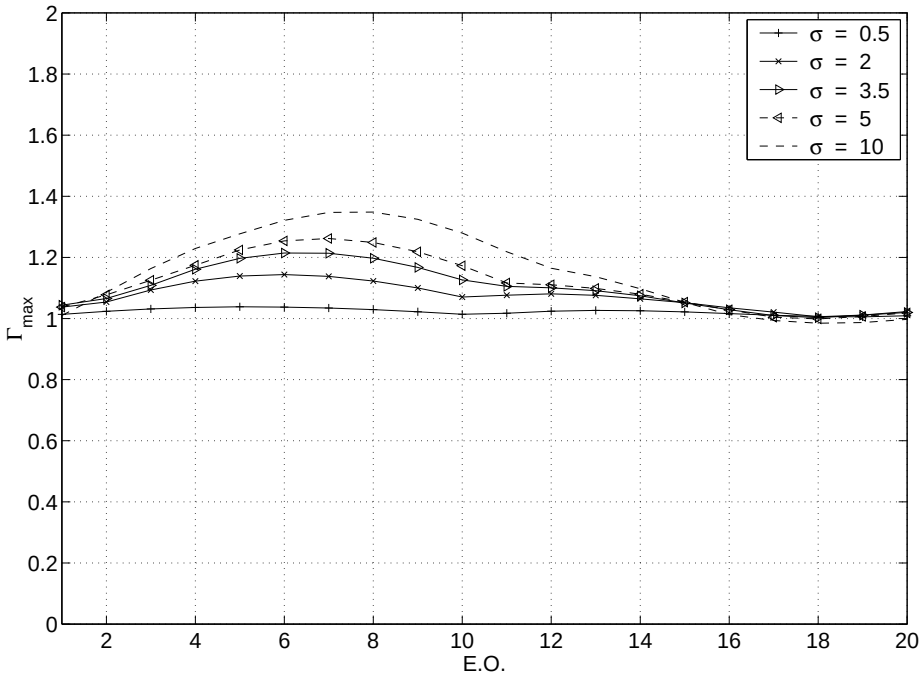

Figure 23: Maximum blade response of randomly mistuned assembly with high level of aerodynamic damping ($b_0 = -8$).